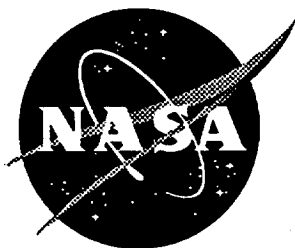NASA Technical Memorandum 110178

Impact Damage Resistance and Residual Property Assessment of [0/±45/90]s SCS-6/Timetal 21S

Jennifer L. Miller
Langley Research Center, Hampton, Virginia

Marc A. Portanova
Lockheed Martin Corporation, Hampton, Virginia

W. Steven Johnson
Georgia Institute of Technology, Atlanta, Georgia

May 1995

National Aeronautics and
Space Administration
Langley Research Center
Hampton, Virginia 23681-0001

IMPACT DAMAGE RESISTANCE AND RESIDUAL PROPERTY ASSESSMENT OF [0/±45/90]S, SCS-6/TIMETAL®21S

Jennifer L. Miller[1], Marc A. Portanova[2] and W. Steven Johnson[3]

Abstract: The impact damage resistance and residual mechanical properties of [0/±45/90]s SCS-6/Timetal®21S composites were evaluated. Both quasi-static indentation and drop-weight impact tests were used to investigate the impact behavior at two nominal energy levels (5.5 and 8.4 J) and determine the onset of internal damage. Through x-ray inspection, the extent of internal damage was characterized non-destructively. The composite strength and constant amplitude fatigue response were evaluated to assess the effects of the sustained damage. Scanning electron microscopy was used to characterize internal damage from impact in comparison to damage that occurs during mechanical loading alone. The effect of stacking sequence was examined by using specimens with the long dimension of the specimen both parallel (longitudinal) and perpendicular (transverse) to the 0° fiber direction. Damage in the form of longitudinal and transverse cracking occurred in all longitudinal specimens tested at energies greater than 6.3 J. Similar results occurred in the transverse specimens tested above 5.4 J. Initial load drop, characteristic of the onset of damage, occurred on average at 6.3 J in longitudinal specimens and at 5.0 J in transverse specimens. X-ray analysis showed broken fibers in the impacted region in specimens tested at the higher impact energies. At low impact energies, visible matrix cracking may occur, but broken fibers may not. Matrix cracking was noted along fiber swims and it appeared to depend on the surface quality of composite. At low impact energies, little damage has been incurred by the composite and the residual strength and residual life is not greatly reduced as compared to an undamaged composite. At higher impact energies, more damage occurred and a greater effect of the impact damage was observed.

Key Words: metal matrix composites, impact, damage, residual strength, residual fatigue

[1]Resident Research Associate, NASA Langley Research Center, MS 188E, Hampton, VA.
[2]Senior Materials Engineer, Lockheed Martin Corporation, Hampton, VA.
[3]Professor of Materials Science and Engineering, Georgia Institute of Technology, Atlanta, GA.

INTRODUCTION

Titanium matrix composites (TMC's) have been candidate materials for high temperature structural applications, such as gas turbine engines, where their high specific strength at elevated temperatures and good general corrosion resistance are beneficial. These materials provide a strong, lightweight alternative to conventional structural alloys due to their ability to maintain mechanical integrity at elevated temperature [1]. Much research has been conducted on the mechanical behavior of TMC's under various types of thermal, mechanical and combined thermomechanical loadings as well as on the various influences of notches and holes [2-7]. However, another critical aspect of the service conditions has received little attention: impact loading. Considerable damage may result from a seemingly innocuous event such as a dropped tool. Characterizing a material's residual properties after impact should be considered in the component design process.

Although several studies have been conducted on polymeric composites [8-11], few studies exist on the impact behavior of continuous fiber metal matrix composites (MMC's). Those studies that do exist are primarily focused on boron fiber reinforced aluminum composites for turbine blade applications. Impact tests on undirectional boron-aluminum composites have shown a considerable reduction in residual strength can occur from low velocity (low energy) impact with a hard object. Carlisle et al. noted a 25% reduction in residual strength at the lowest impact velocity used in the study [12]. When residual fatigue of the boron/aluminum composites was considered, at the slowest test velocity, Gray found the fatigue life was reduced by an order of magnitude [13]. In both studies, the residual properties continued to decrease as impact velocity, and consequently impact energy, increased. Comparisons to unreinforced titanium alloys in the previously mentioned studies showed the boron/aluminum composites to be less damage resistant and less damage tolerant than the monolithic material.

Similar impact studies conducted on polymer matrix composites (PMC's) show distinctive differences in the damage mechanisms occuring in these materials as compared to MMC's (delamination versus fiber/matrix cracking); however, some general trends of the PMC behavior may

2

apply to MMC's. Greszczuk found cross ply laminates resist impact damage better than undirectional or psuedoisotropic laminates [11] when investigating PMC's. Another trend noted in Greszczuk's study was that damage resistance increased when a stronger matrix material is used. Since the strength of a metal can be varied easily through heat treatment, this effect could apply to MMC's. The differences in damage resistance occuring in PMC's due to variations in laminate layup and constituent elastic properties may also apply to MMC's.

In this study the impact resistance and residual mechanical properties of quasi-isotropic SCS-6/Timetal®21S composites is evaluated. The onset of internal damage is described in terms of impact energy. Residual strength and residual fatigue tests were conducted at room temperature and the results are compared to those of non-impacted materials. The influence of prior impact on fracture behavior and damage acculumation is also examined.

MATERIALS AND PROCESSING

The SCS-6/Timetal®21S composites tested were manufactured into [0/±45/90]s quasi-isotropic laminates by hot isostatically pressing thin foils of Ti-15Mo-3Nb-3Al-0.2Si (Timetal® 21S) between unidirectional tapes of SCS-6 silicon carbide fibers. The 0.14 mm diameter fibers were held in place by crosswoven Ti-Nb wires. Several laminates of varying thicknesses between between 1.70 to 1.88 mm were used in this study. Several sections were examined to determine any variation in fiber spacing and the average fiber volume fraction. Of the laminates examined, those with the smaller nominal thickness showed a greater variation in fiber spacing. The average fiber volume fraction for the laminates ranged from 0.348 to 0.357. Figure 1 displays photomicrographs of the polished cross sections of two laminates. As shown, the average fiber spacing (0.216 mm) did not vary greatly in the thicker panels (Figure 1a), whereas there is a much greater variation in thin panels (Figure 1b).

Of the various laminated sheets from which specimens were manufactured many variations in quality occur, both internally and on the exterior surfaces of the sheets. The photograph and radiograph of two different specimens in Figure 2 illustrates some of these defects. Fiber swim

3

describes the waviness in the fibers as indicated in the figure. Fish eyes are areas where the fibers separate and rejoin, forming a gap. Both of these defects contribute to non-unifrom fiber spacing throughout the composite. The laminates were examined prior to machining to determine the best arrangement to use to machine the impact specimens to avoid placing theses defects in the center of a specimen. However, the defects could not be avoided altogether.

The 152 mm X 102 mm impact specimens were machined using a diamond-impregnated abrasive cutting wheel. The long dimension of the panel was oriented both parallel and prependicular to the 0° fiber direction, yielding two different panel designations and layups: the original $[0/\pm45/90]_s$ are the longitudinal specimens and the 90° rotated orientation yields a $[90/\pm45/0]_s$ layup for the transverse specimens. By varying the panel orientation, the effects of stacking sequence on mechanical behavior could be examined. Prior to heat treating, specimens were degreased and chemically cleaned using a diluted mixture of hydrofluic and nitric acid followed by a dilute hydrochloric acid wash. The specimens were then subjected to a β-stabilization heat treatment consisting of an eight hour soak in vacuum at 620° C to prevent α precipitation during future elevated temperature testing [14]. All specimens were examined radiographically and by ultrasonic C-scan both prior to and after impact testing to assess the damage state of the specimens. The results will be discussed in a later section.

After the impact tests were completed, 152 mm X 25.4 mm specimens were machined from the damaged panels for residual property evaluation. The entire impact area was contained within the cross sectional area of these specimens. Some permenant bending deformation may have occured in some specimens due to the impact event. Strain gages were applied to the back and front surface of these specimens along the centerline to determine the magnitude of the initial bending stress applied when the specimens straightens during placement in the grips of the testing machine. Several other 152 mm X 12.5 mm specimens were machined from the edges of the panels for use in baseline tension and constant amplitude fatigue studies. End tabs were applied to all specimens with cyanoacrylate adhesive to reduce the gripping stress and prevent specimen failure in the grip sections. Table 1 describes the residual property test matrix used in the study.

4

EXPERIMENTAL PROCEDURE

Impact Tests

Two different test methods were employed to assess the damage resistance of the TMC's: quasi-static indentation (QSI) and drop-weight impact (DWI) [8]. Two impact energies, 5.4 J (4.0 ft-lbf) and 8.4 J (6.2 ft-lbf) were recommended by industry as energies typical of tool drops. The QSI tests were performed using a servo-hydraulic test frame at a constant displacement rate of 0.51 mm/min. During testing the specimens were clamped firmly in an aluminum test fixture that contained a 127 mm by 76.2 mm opening with corner radii of 12.7 mm. An instrumented tup attached to a 12.7 mm diameter hemispherical indenter was used to measure load. The tup was mounted in the grips of the load frame such that the indenter traveled normal to the plane of the specimen. The indentation load and stroke output were recorded at a rate of one data point per second throughout the loading history using a digital storage oscilloscope.

Drop-weight impact tests were conducted using the same instrumented tup and test fixture as in QSI tests, resulting in the same plate boundary conditions. The total free falling mass of the indentor, tup and steel weight was 3.03 kg. The impactor was centered above the panel at the required height to impart the desired impact energy. After the impactor struck the specimen, a dummy panel was quickly moved between the fixture and specimen to prevent multiple impacts. The impact force-time history was then recorded in real time using a digital storage oscilloscope.

Residual Property Tests

The room temperature tension and constant amplitude fatigue tests were conducted in a 100 kN closed loop servo-hydraulic test frame equipped with hydraulic grips. A 7 MPa gripping pressure was used in all tests. Tension tests were conducted in stroke control at a rate of 1.27 mm/min. Constant amplitude fatigue tests were conducted in load control using a sinesoidal waveform at a frequency of 1 Hz and an R-ratio of 0.1. The bending stress induced when gripping the damaged specimens was measured using 350 Ω electrical resistance strain gages mounted to the front and back face of the specimens, oriented longitudinally and transversely with

respect to the gage length, and positioned 25.4 mm above and below the damage area. The measured strains were small in comparison to the applied loads and did not appear to influence the results greatly. Axial strain during loading was measured using a strain gage extensometer with a 25.4 mm gage section. Baseline data for both tension tests and constant amplitude fatigue tests were generated by testing the undamaged coupons cut from the edges of the impact panels.

RESULTS AND DISCUSSION

Impact Damage Resistance

The impact damage resistance of the TMC's was evaluated by examining the force versus displacement response of the panels when subjected to both quasi-static indentation (QSI) and drop-weight impacts (DWI). The energy applied during loading was calculated by integrating the force versus displacement curves. Two nominal impact energies, 5.4 J and 8.4 J, were sought throughout the study when comparing results since slight variations occur in the impact energy for each individual panel tested. Figures 3 and 4 compare the TMC's response to QSI and DWI tests at 8.4 J for longitudinal and transverse specimens, respectively. The oscillation in the force-displacement response of the DWI test is due to vibrations that occur as the incident wave reflects off the clamped plate boundaries. The vibration is inherent in the test method [8]. The response of the TMC's to both types of tests was similar: as the contact force on the panel increases, the displacement of the panel increases, and subsequently, the applied energy increases. If the contact force is increased enough, strain will accumulate in the composite until reaching the fiber failure strain wherein the fibers break. When this occurs the contact force decreases rapidly since the dominant load carrying component of the composite is damaged. Matrix cracking usually proceeds fiber failure as shown in past studies on the mechanical response of TMC's [2-4]. Since there was no significant difference between the force-displacement response of the panels subjected to QSI or DWI, the QSI was determined to be the best method of testing the impact resistance. This method provided a repeatable test that allowed the contact force to be increased slowly, thereby permitting the test to be interrupted periodically to examine the specimen to determine if any damage was visible.

6

The impact results for all the longitudinal and transverse specimens show the mean value of the first load drop occurs at 4.5 kN. The first load drop indicates that damage has occurred and are identified on Figures 3-5. The mean applied energy corresponding to this mean load drop is 6.3 J and 5.0 J for the longitudinal and transverse specimens, respectively. The difference in applied energy at initial load drop may be due in part to the variation in the bending stiffnesses of the two different stacking sequences. Figure 5 compares a typical response for a longitudinal and a transverse specimen subjected to a nominal 8.4 J QSI. The transverse specimen is stiffer in bending since the fibers in the outer ply span the short dimension of the rectangular plate during loading. As shown in Figure 4, in order to produce the same amount of deflection of the plate, a greater force must be applied to the transverse specimens. Although there is a difference in the energy at the first load drop, it is within the statistical variation of the test results. Figure 6 is a histogram displaying the mean energy associated with the first load drop as well as the maximum and minimum values for each specimen orientation. The numbers above the bars indicate the number of specimens used to determine the mean while the error bars represent one standard deviation above and below the mean. The range of energies for both orientations overlap. Since there were several composite sheets from which specimens were made, all having slight differences in the surface quality, degree of fiber swim and in other manufacturing anomolies, the resulting variations in mechanical response would be expected.

When examining the panels tested at the lower energy levels, a few displayed matrix cracks; however, x-rays did not show internal fiber breaks occurring. All the longitudinal panels tested showed internal damage when subjected to a forces greater than 4.1 kN or at energies above 5.6 J. Similar results are obtained for the transverse panels for forces greater than 3.6 kN or at 3.9 J. The matrix cracking on the backface of the panels tested at low energies (lower than the mean energy associated with the first load drop) indicates that the appearance of visible damage does not give a clear indication of the true damage state of the material. Matrix cracking on the surface does not imply fiber breakage in the interior. Although, at higher energies, when fibers are broken, matrix cracking also occurs. The development of matrix cracks prior to the first load drop in the

force-displacement response suggests that the first load drop is characteristic of fiber damage occuring within the composite and not due to the matrix cracking.

Damage Assessment

Damage varied greatly in both specimen orientations depending on the impact energy. Longitudinal and transverse matrix cracks and broken fibers were found at the higher impact energies. Crack lengths were measured on the surface of the specimens and from radiographs. The exterior surface cracks were in general longer than those shown on the radiographs. Table 2 shows the surface crack measurements and the interior (x-ray) crack measurements for cracks running in the longitudinal and transverse plate directions as a function of impact energy. There is a considerable amount of scatter in the data. As mentioned previously, in some of the specimens tested at low energies, no fiber breaks were found by radiography. The extent of the damage incurred by the TMC's appears to be sensitive to the quality of the laminate due to the stress concentrations produced by non-uniform fiber distributions. This sensitivity to manufacturing defects was suspected when specimens undergoing residual fatigue tests did not fail at the impact site. These results will be discussed in the next section. Ultrasonic C-scan inspections did not provide any further insight into the extent of damage due to the local permenant deformation at the contact site compounded by the bending deformation of the panels. The bending displacement caused a change in signal attenuation that could not be discerned from the attenuation due to internal damage. Unlike polymer matrix composites, where large delaminations occur due to impact [10], the C-scan doesn't provide a method of quantifying damage in the TMC.

Residual Property Assessment

Residual Strength--A comparison of the results from selected tension tests on both non-impacted and impacted longitudinal specimens are shown in Figure 7. During the residual tension tests, failures occurred in the damage area for all but one specimen which failed in the grip area. Results for the transverse specimens were similar to those of the longitudinal specimens. From the

stress-strain response the initial elastic modulus, the 0.2% offset yield stress, the ultimate strength and the failure strain of the composites were determined and are given in Table 3. Figures 8-11 are histograms representing the mean values of these properties as a function of nominal impact energy. The error bars displayed on each of these figures represent one standard deviation above and below the mean for each property while the numbers above each bar give the number of tests.

Figure 8 compares the mean initial elastic moduli (E_I) of non-impacted and impacted materials for both specimen orientations. The elastic modulus was determined from the initial loading portion of the curve prior to the knee that occurs at approximately 200 MPa. The elastic response for the longitudinal and transverse specimens were similar. For impacted specimens the E_I's fall within the range shown by the error bars for the undamaged materials. The impact event does not appear to have caused considerable fiber-matrix debonding that would have otherwise resulted in a reduced elastic modulus. The presence of local matrix cracks would not be expected to change a global property like E_I. Similarly, the prior impact does not seem to influence the 0.2% offset yield stress (σ_y) as shown in Figure 9. During a few of the tests insufficient yielding occured and σ_y could not be determined. Table 3 displays the test conditions during which the insufficient yielding occurred. The bars of histogram in Figure 9 is labeled with the number of tests used to calculate the mean 0.2% offset yield stress. The lower failure strain for the impacted specimens can be attributed to a local effect of the impact damage on the fracture behavior of the material. As shown in Figure 10 and 11, the mean ultimate strength (σ_u) and the mean failure strain (ε_f) are reduced for the impacted specimens. The premature failures are due to the local effect of the impact damage, not simply a net section effect. The damage increases the fiber stresses locally, causing fibers to begin to fail at lower applied (global) stresses. This results in a reduction in the global (applied) ultimate stress. The reduction in ε_f (measured globally) is also attributed to local stress increase in the fibers. Both the longitudinal and transverse specimens tested at the 8.4 J impact energy showed a greater decrease in σ_u and ε_f than those tested at 5.4 J. These specimens also suffered the most severe damage, fiber breaks and matrix cracks. The tension test results for

9

the longitudinal and transverse specimens were very similar; the variation in the stacking sequence did not seem to influence the tensile response of the TMC's examined.

Since residual properties are a concern of this study, the mean ultimate strength for the impacted materials was normalized with respect to the mean ultimate strength for the undamaged materials. This will result in a relative measure of the material's damage tolerance. Figure 12 shows the normalized residual strengths as a function of impact energy for both specimen orientations. The results show that low energy impacts, where little damage is incurred by the composite, did not greatly effect the strength of the material. In particular, when only matrix cracking occurred, the residual strength was within the statisical variation of the undamaged material strengths. The mean residual strength for a 5.4 J impact is 95% of the mean ultimate for undamaged materials. As as the amount of fiber damage increased, the retention of composite strength decreased. For the 8.4 J impact, the residual strength is effectively reduced on average by 20%.

Baseline Fatigue Study--Constant amplitude fatigue tests were conducted on undamaged specimens to establish a baseline for assessing the residual life of impact damaged materials. Both longitudinal and transverse specimens were tested to determine if the laminate layup affected the fatigue life of the materials. Figure 13 displays the results of the baseline tests. Each data point represents one specimen. A run out criterion of 10^6 cycles was used to set an endurance limit for the material and is indicated by the arrows shown in the figure. Both specimen orientations showed similar fatigue lives at the applied stress levels tested with the transverse specimens typically having a longer life. In terms of overall fatigue life, little effect of laminate layup is shown.

A longtiudinal specimen tested at 310 MPa and a transverse specimen tested at 276 MPa failed at much lower fatigue lives than the other tests. Both of these specimens were from the thinner panels (1.7 mm). X-rays showed non-uniform fiber distributions and a considerable amount of fiber swim in comparison to the other panels tested. Figure 1 showed a typical cross section of the material from which the transverse specimen was machined. As discussed

previously, the fiber spacing varied greatly through the thickness of this material. Stress concentrations due to the higher fiber density may have increased matrix cracking and produced a higher net section stress, increasing strain accumulation leading to composite failure. Although the thinner composites had similar strengths to other composites in tension, the local effect of fiber spacing would be more significant in fatigue where crack propagation is greatly influenced by local stress fields in the material.

Residual Fatigue Life--The results of the fatigue tests on impacted specimens are shown in Figure 14 along with the baseline fatigue results for two applied stresses. There is considerable variation in the residual fatigue lives of the impacted specimens. For the longitudinal specimens tested at 345 MPa, the trend is as expected--the higher the impact energy, the more initial damage and the shorter residual fatigue life. However, the longitudinal specimen impacted at 5.4 J did not have any fiber breaks. The specimen did have substantial fiber swim, particularly in the 0° surface plies. Since no fiber breaks occurred, a fatigue life similar to an undamaged specimen would be expected (for the same test conditions). As the results show, the fatigue life was much lower than the undamaged composite. The specimen also failed outside of the impacted region. X-rays show a large gap separating 0° fibers where only matrix is found. By examining the fracture surface, it was determined that in this area where only the matrix exists, there should be approximately 15 fibers. The fiber gap essentially reduces the total number of 0° fibers in the composite by approximately 5%. Since the 0° fibers are the dominant load carrying component in the composite, reducing their number may have contributed to the reduced fatigue life. The 0° fibers also bridge fatigue cracks occuring in the composite resulting in slower fatigue crack growth [3-5]. Similarly, the undamaged specimen tested at 414 MPa had a shorter life than the impacted specimens. Again x-rays show substantial fiber swim and several fisheyes occuring along the length of the specimen. When comparing the results for the specimens impacted at 8.4 J little difference is shown for the two applied stress levels. The specimen tested at 345 MPa had a longer transverse crack length and may have suffered more internal damage initially, causing a reduction in fatigue life. The

11

amount of impact damage from the 8.4 J tests varied a great deal, so it would be expected that the residual fatigues lives would also vary considerably.

Little difference is shown in the fatigue results at 345 MPa between the undamaged transverse specimen and the one impacted at 5.4 J where no fiber breaks occurred. The longer life may be typical of the statistical variation of this material's properties. The 8.4 J impact had a very short life in comparison, but may be due to a finite width effect. The specimen had a large transverse crack with respect to its width and did not give a true indication of the material's damage tolerance due to the greatly reduced cross section. The results for the 414 MPa tests showed the expected trend, as discussed previously. The 5.4 J impacted specimen had a similar life to the undamaged specimen. No fiber breaks occurred in this specimen. The 8.4 J impact specimen had a small transverse crack and as shown, its residual fatigue life was reduced.

The variation in the fatigue lives and the location of failures with respect to manufacturing anomolies, seems to indicate variations in mechanical properties are dependent on the quality of the laminate. These defects are more damaging to the composite than low energy impacts. Although there is considerable variation in the test results, the general trend of reduced life with an increasing amount of initial damage has been shown. Figure 15 shows the initial crack lengths (longitudinal and transverse) measured on x-rays compared to the fatigue life for each specimen tested. The solid vertical lines represent the average fatigue lives for the two applied stresses shown. The longitudinal crack length doesn't appear to influence fatigue life; however, as the initital transverse crack length gets longer, the residual fatigue life decreases.

Fractography--Fracture surfaces of the specimens from the baseline constant amplitude fatigue (CAF) tests and the residual fatigue tests were examined using a scanning electron microscope (SEM). Micrographs of a non-impacted specimen subjected to CAF at 345 MPa is shown in Figure 16. A step-like fracture surface occurs (Figure 16a), typical of this type of TMC [15], indicating fatigue crack initiation at multiple sites within the material. Fatigue crack growth is controlled by crack initiation at debonded fiber/matrix interfaces on off-axis plies. Figure 16b

12

shows multiple initiation sites occurring along a 45° fiber. Final fracture occurs via ductile rupture as indicated by the equiaxed dimples shown in the matrix of the 0° ply adjacent to this 45° ply. This type of fracture behavior has been identified in other angle ply TMC's [15]. None of the specimens tested that were previously subjected to the nominal 5.4 J impact showed any initial fiber breakage in x-rays. Of these specimens, three did not fail in the impacted area. The fracture surfaces of those specimens were no different from those that were not impacted. As discussed earlier, they did fracture along areas where fiber swim can be seen on the outside surface of the specimen.

Figure 17 shows a longitudinal specimen impacted at the nominal 8.4 J energy. The fracture surface was tilted to show the longitudinal matrix crack running in the 0° ply. The initial transverse crack that appears on x-rays traverses the entire thickness of the specimen, as pointed out in Figure 17a, breaking the off axis fibers, but running around the 0° fibers, causing debonding. Figure 17b is a magnified view of the cross section showing the crack running around the 0° fiber and propogating into the 45° ply. Note that the 0° fiber is broken in a different plane than the matrix, indicating fiber pullout during final fracture. The matrix around the 0° fiber also shows ductile rupture. Away from the damage area, the fracture surface is similar to the undamaged material. In reviewing the residual fatigue results, the presence of transverse cracks in the TMC's do not appear to alter the mechanism of crack growth, but provide a larger initial damage area for crack propogation. The initial crack adds to the numerous small fatigue cracks growing from debonded fibers to accumulate sufficient strain to fail the composite.

CONCLUSIONS

The impact damage resistance of [0/±45/90]s SCS-6/Timetal®21S composites was evaluated experimentally using both quasi-static indentation and drop-weight impact tests. Longitudinal and transverse specimens were tested to examine the effect of stacking sequence. Results showed that the quasi-isotropic TMC's were able to resist impact damage when subjected to a contact force of 4.5 kN corresponding to impact energies of 6.3 J and 5.0 J for the longitudinal and transvese

specimen orientations, respectively. The difference in the impact energy associated with the onset of damage is due to the greater plate bending stiffness for the transverse specimen orientation. The extent of the damage incurred by the TMC's was evaluated non-destructively through x-ray inspection. At higher impact energies fibers were broken and residual properties were affected. Both the residual tensile strength and residual fatigue life as a function of impact energy were evaluated. The composites were able to withstand 5.4 J impacts without a substantial loss of tensile strength or fatigue crack growth resistance. At higher impact energies, the initial impact damage affects these properties more greatly. Results showed that matrix cracking alone is not sufficient to reduce tensile strength or fatigue life. Only when fibers are broken are the TMC's tensile strengths and failure strains reduced. The initial elastic modulus and 0.2% offset yield stress are not affected by the impact damage. The TMC's impacted nominally at 5.4 J had a residual tensile strength of 95% of the undamaged strength whereas the those impacted at 8.4 J had 80% of the non-impacted strength. The variation in fatigue life and the location of failure with respect to manufacturing anomolies, seems to indicate variations in mechanical properties are dependent on the quality of the laminate; the defects are more damaging than the low energy impacts. Although there is considerable variation in the test results, the general trend of reduced life with an increasing amount of initial damage has been shown. The presence of initial longitudinal cracks doesn't appear to influence fatigue life; however, as the initital transverse crack length gets longer, the residual fatigue life decreases. From examination of the fracture surfaces, the presence of transverse cracks in the TMC's appears not to alter the mechanism of crack growth, but provides a larger initial damage area for crack propogation. The initial crack adds to the numerous small fatigue cracks growing from debonded fibers to accumulate sufficient strain to fail the composite.

REFERENCES

1. Smith, P.R., and Froes, F.H. , "Developments in Titanium Metal Matrix Composites," *Titanium Technology: Present Status and Futures Trends*, Titanium Development Association, Dayton, 1985, pp. 157-164.

2. Mirdamadi, M., Johnson, W.S., Bahei-El-Din, Y.A., and Castelli, M.G. "Analysis of Thermechanical Fatigue of Unidirectional Titanium Metal Matrix Composites," *Composite Materials: Fatigue and Fracture, Fourth Volume, ASTM STP 1156*, W. W. Stinchcomb and N.E. Ashbaugh Eds., American Society for Testing and Materials, Philadelphia, 1993, pp. 591-607.

3. Bakuckas, J.G., Jr., Johnson, W.S., and Bigelow, C.A., "Fatigue Damage in Cross-Ply Titanium Metal Matrix Composites Containing Center Holes," *NASA TM-104197*, NASA Langley Research Center, 1992.

4. Herrmann, D.J., Ward, G.T., Lawson, E.J., and Hillberry, B.M., "Prediction of Matrix Fatigue Crack Initiation From Notches in Titanium Matrix Composites," *Life Prediction Methodology for Titanium Matrix Composites, ASTM STP 1253*, W.S. Johnson, J.M. Larsen, and B.N. Cox, Eds., 1995.

5. Larsen, J.M., Jira, J.R., John, R., and Ashbaugh, N.E., "Crack Bridging Effects in Notch Fatigue of SCS-6/Timetal®21S Composite Laminates," *Life Prediction Methodology for Titanium Matrix Composites, ASTM STP 1253* W.S. Johnson , J.M. Larsen and B.N. Cox, Eds., American Society for Testing and Materials, Philadelphia, PA.

6. Castelli, M.G., Bartolotta, P.A., and Ellis, J.R., "Thermomechanical Fatigue Behavior of SiC (SCS-6)/Ti-15-3," *Composite Materials: Testing and Design (Tenth Volume), ASTM STP 1120*, Glen C. Grimes, Ed., American Society for Testing and Materials, Philadelphia, 1991, pp.70-86.

7. Russ, S.M., Nicholas, T., Bates, M., and Mall, S., "Thermomechanical Fatigue of SCS-6/Ti-24Al-11Nb Metal Matrix Composite," *Failure Mechanisms in High Temperature Composite Materials, ASME, AD-Vol. 22/AMD Vol. 122*, American Society of Mechanical Engineers, New York, 1991, pp. 37-43.

8. Poe, C.C., Jr., Portanova, M.A., Masters, J.W., Sankar, B.V., and Jackson, W.C., "Comparison of Impact Results for Several Polymeric Composites over a Wide Range of Low Impact Velocities," *NASA CP-3104*, NASA Langley Research Center, 1990.

9. Jackson, W. C., and Poe, C. C. Jr., "The Use of Impact Force as a Scale Parameter for the Impact Response of Composite Laminates," *Journal of Composites Technology & Research*, Vol. 15, No. 4, 1993, pp. 282-289.

10. Portanova, M.A., Poe, C.C., Jr., and Whitcomb, J.D., "Open Hole and Post-Impact Compression Fatigue of Stitched and Unstitched Carbon / Epoxy Composites", *Composite Materials: Testing and Design (Tenth Volume,) ASTM STP 1120*, American Society for Testing and Materials, Philadelphia, 1992, pp.37-53.

11. Greszczuk, L.B., "Damage in Composite Materials Due to Low Velocity Impact," *Impact Dynamics*, John Wiley & Sons, New York, 1982, pp. 55-94.

12. Carlisle, J.C., Crane, R.L., Jaques, W.J., and Montulli, L.T., "Impact Damage Effects on Boron-Aluminum Composites," *Composite Reliability, ASTM STP 580*, American Society for Testing and Materials, Philadelphia, 1975, pp. 458-470.

13. Gray, T.D., "Foreign Object Damage and Fatigue Interaction in Unidirectional Boron/Aluminum-6061," *Fatigue of Composite Materials, ASTM STP 569*, American Society for Testing and Materials, Philadelphia, 1975, pp. 262-279.

14. Data Sheet for Timetal®21S (Ti-15Mo-3Nb-3Al-0.2Si) High Strength, Oxidation Resistant Strip Alloy, Timet Corp., Denver, CO.

15. Johnson, W.S., Miller, J.L., and Mirdamadi, M., ""Fractographic Interpretation of Failure Mechanisms in Titanium Matrix Composites," TMS/ASM Symposium on *Mechanisms and Mechanics of MMC Fatigue*, Oct. 2-6, 1994, Rosemont, IL.

Table 1--Residual property test matrix.

Specimen ID	Nominal Impact Energy, Joules	Residual Property Test Method
91L01D	5.4	tension
99L01D	5.4	tension
90L04D	8.4	tension
92L01D	8.4	tension
118L01D	8.4	tension
95T03D	5.4	tension
96T01D	5.4	tension
48T01D	8.4	tension
99L03D	5.4	345 MPa CAF[a]
92L03D	5.4	414 MPa CAF
90L05D	8.4	345 MPa CAF
92L05D	8.4	414 MPa CAF
95T04D	5.4	345 MPa CAF
98T02D	5.4	414 MPa CAF
93T04D[b]	8.4	345 MPa CAF
95T02D	8.4	414 MPa CAF

[a] Constant Amplitude Fatigue
[b] 12.7 mm wide specimen

17

Table 2--Comparison of crack length measurements for impacted specimens.

Specimen ID	Nominal Impact Energy Joules	Surface Measurements		X-ray Measurements	
		Longitudinal Crack mm	Transverse Crack mm	Longitudinal Crack mm	Transverse Crack mm
91L01D	5.4	7.14	3.13	7.14	---
99L01D	5.4	1.63	2.77	---	---
90L04D	8.4	7.95	4.78	7.94	4.78
92L01D	8.4	7.69	4.51	7.54	3.18
118L01D	8.4	5.94	5.56	4.37	4.76
95T03D	5.4	8.26	4.11	7.94	3.18
96T01D	5.4	7.95	17.85	7.94	17.86
48T01D	8.4	11.93	6.20	11.91	5.94
99L03D	5.4	6.47	1.28	a	---
92L03D	5.4	4.81	---	---	---
90L05D	8.4	8.78	4.80	7.94	3.57
92L05D	8.4	3.77	0.617	2.78	---
95T04D	5.4	2.84	3.43	---	---
98T02D	5.4	---	---	---	---
93T04D[b]	8.4	7.37	5.59	7.13	3.96
95T02D	8.4	16.28	4.91	16.28	3.18

a not available
b 12.7 mm wide specimen

Table 3--Residual tension results.

Specimen ID	Nominal Impact Energy, Joules	Initial Elastic Modulus, GPa	0.2% Offset Yield Stress, MPa	Ultimate Strength MPa	Failure Strain
91L01D	5.4	17.95	a	146.59	0.00916
99L01D	5.4	21.20	104.90	123.30	0.00902
90L04D	8.4	18.60	a	98.34	0.00706
92L01D	8.4	22.79	109.07	131.79	0.00923
118L01D	8.4	19.30	99.04	112.69	0.00936
95T03D	5.4	21.34	108.55	143.36	0.1092
96T01D	5.4	17.70	116.00	118.98	0.00894
48T01D	8.4	21.62	99.50	112.63	0.00799

[a] Insufficient yielding to calculate the 0.2% offset yield stress.
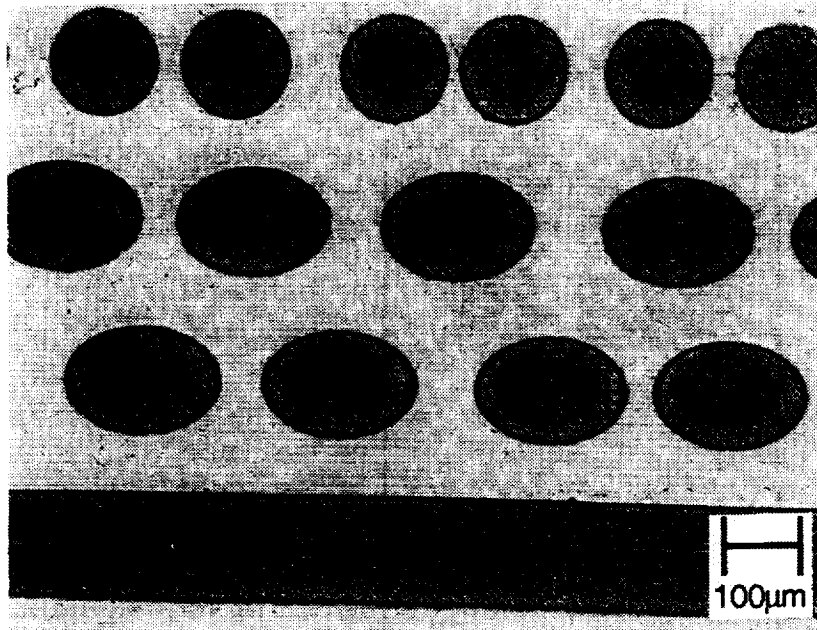
(a) Typical cross section representing 1.80-1.88 mm thick specimens
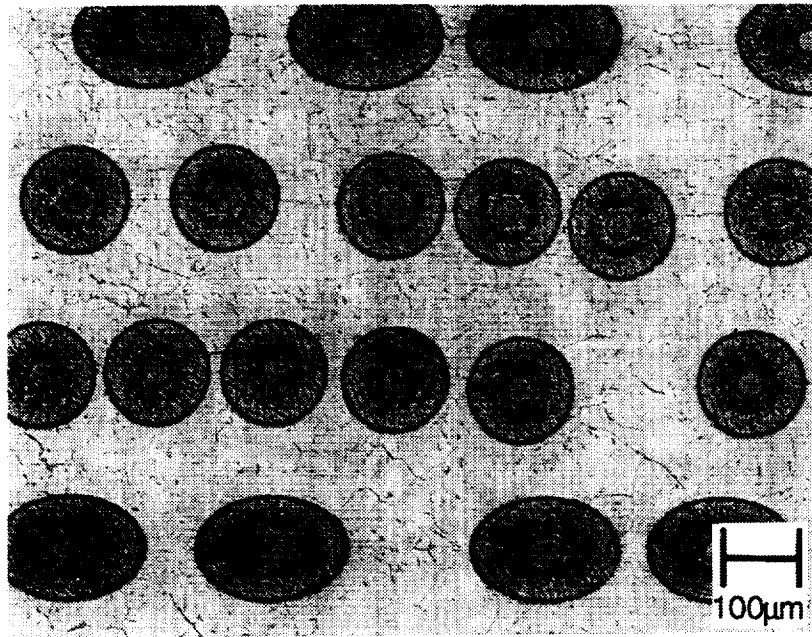
(b) Typical cross section representing 1.70 mm thick specimens

Figure 1.   Optical micrographs of [0/±45/90]$_S$ SCS-6/Timetal®21S laminates; a) typical cross section representing specimens having thickness ranging from 1.80 to 1.87 mm and b) typical cross section representing specimens of 1.70 mm thickness.

20

FIBER
SWIM

FISHEYE
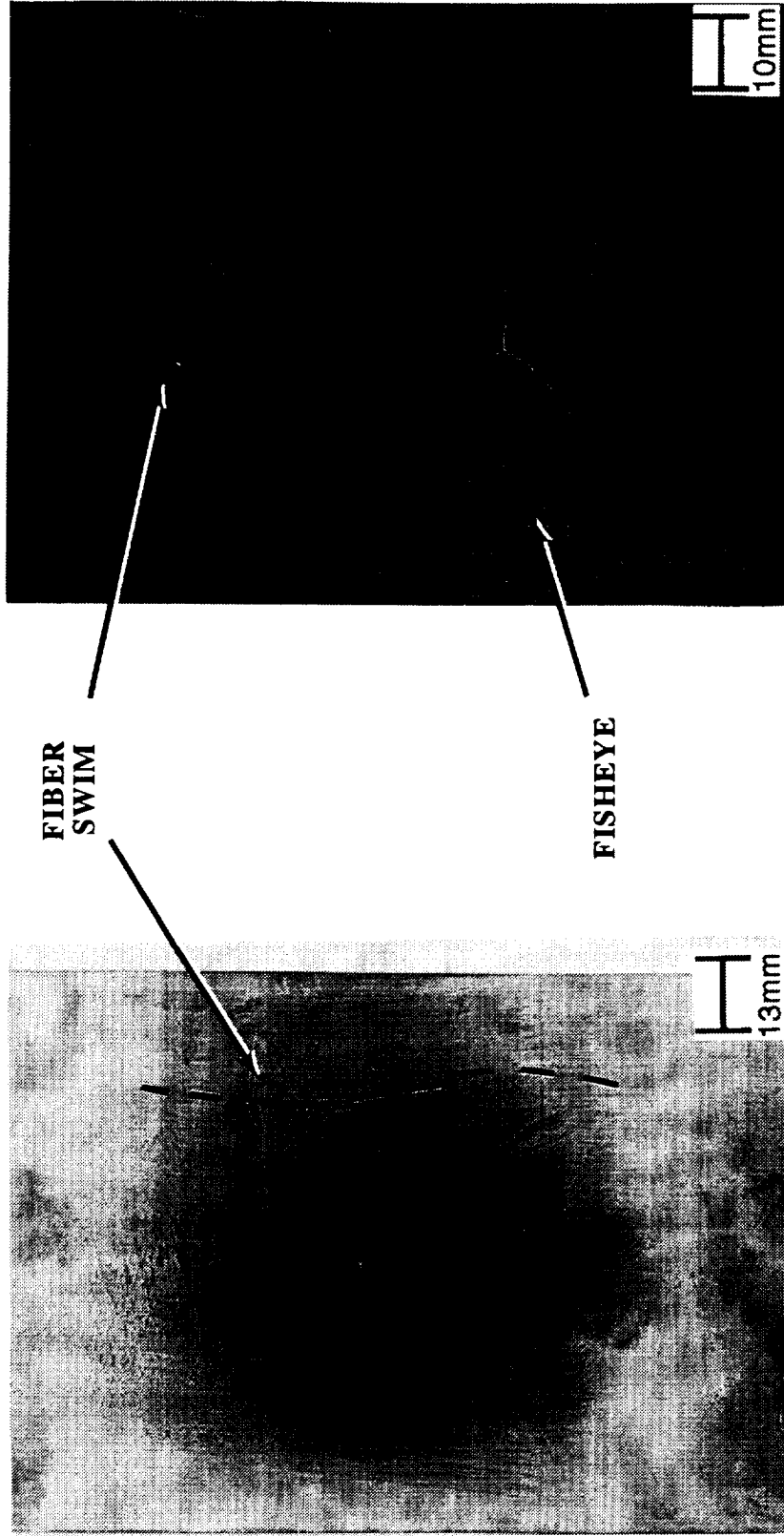
(a) Specimen surface

10mm

13mm

(b) Interior surface

Figure 2.   Variations in manufacturing quality of [0/±45/90]s SCS-6/Timetal®21S composites; a) photograph of an impact panel showing surface roughness and fiber swim; b) radiograph of an impact panel showing fisheyes and fiber swim.
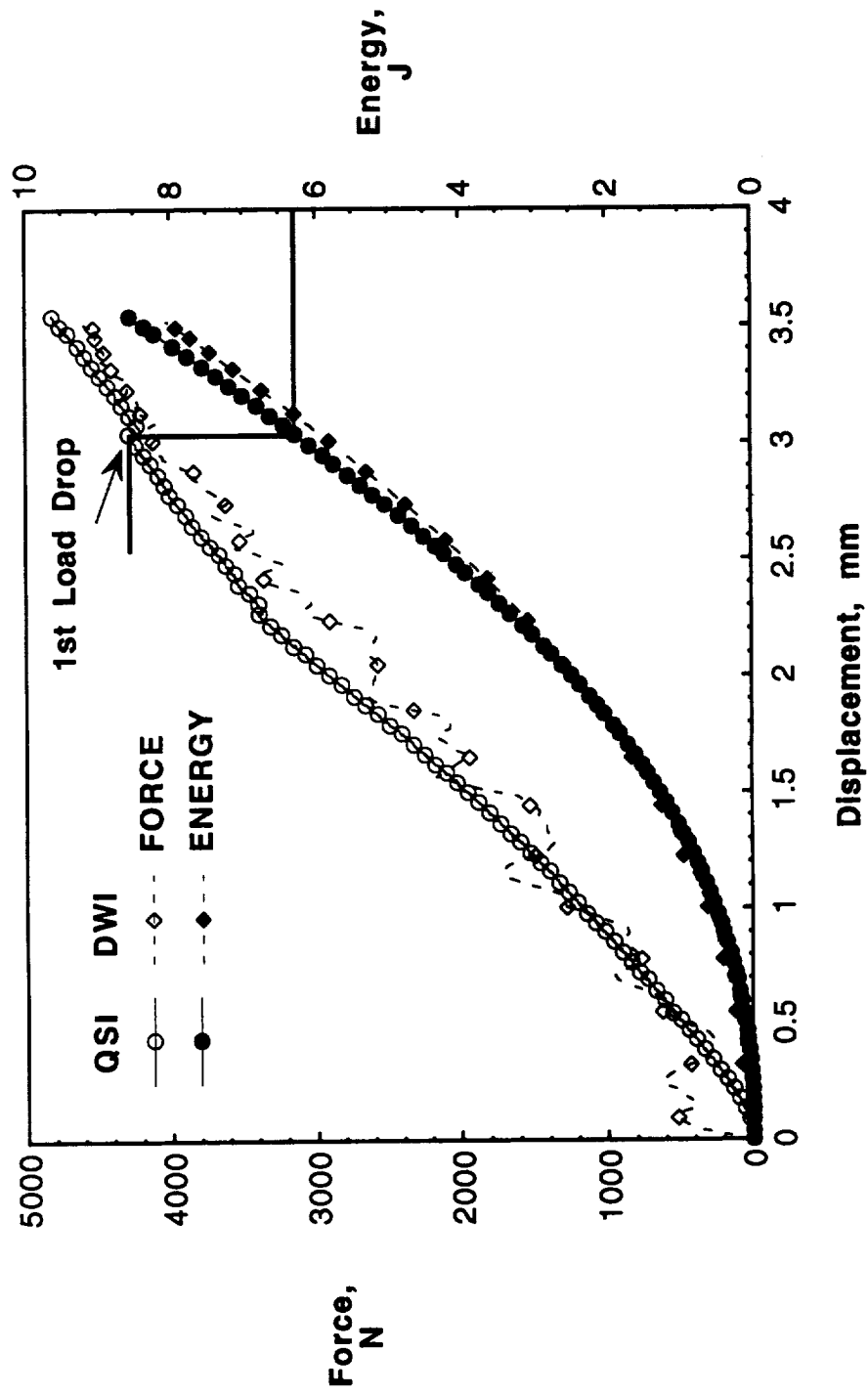
Figure 3. Comparison of the response of longitudinal [0/±45/90]s SCS-6/Timetal®21S to quasi-static indentation (QSI) tests and drop-weight impact (DWI) tests.
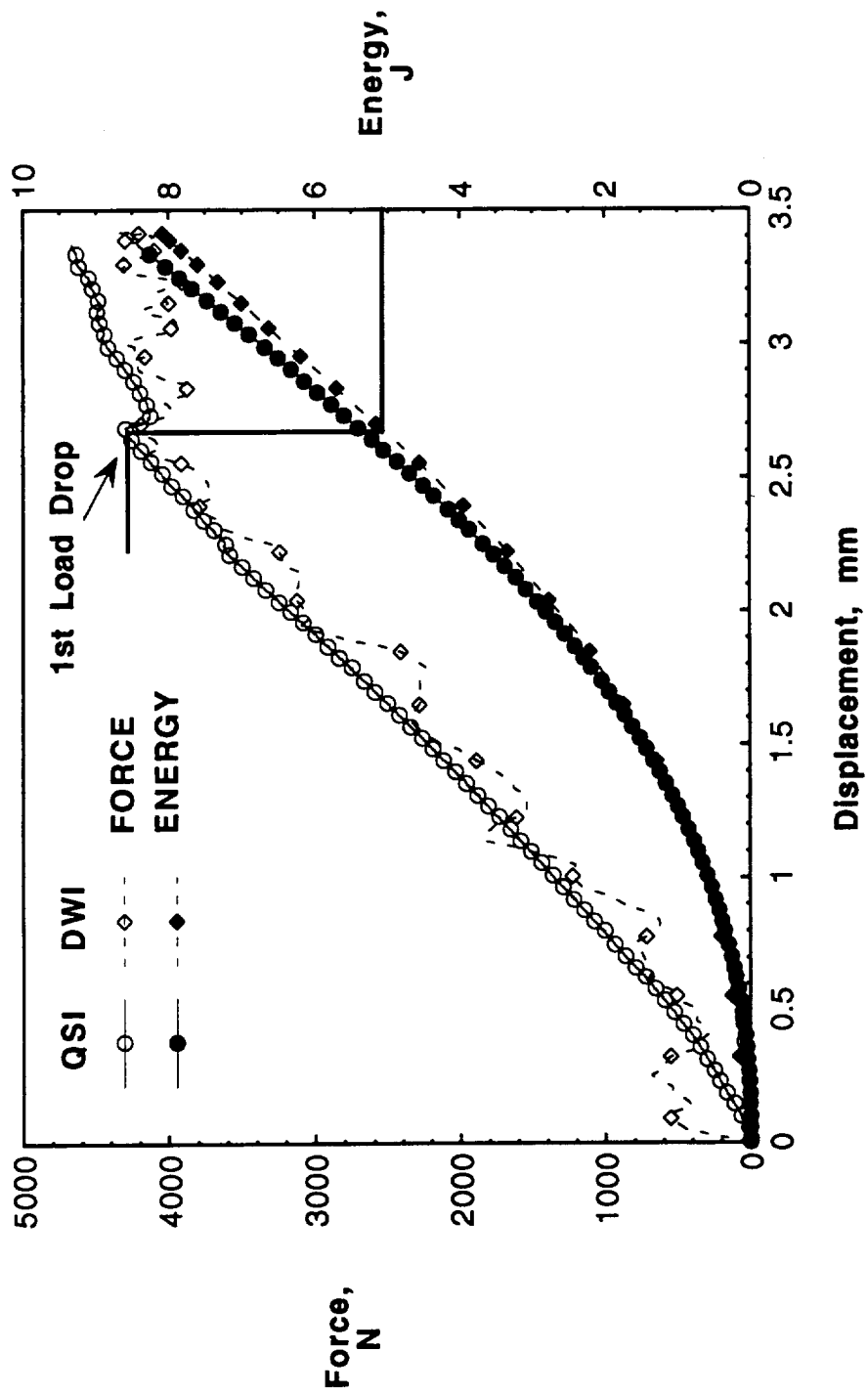
Figure 4.   Comparison of the response of transverse [90/±45/0]s SCS-6/Timetal®21S to quasi-static indentation (QSI) tests and drop-weight impact (DWI) tests.
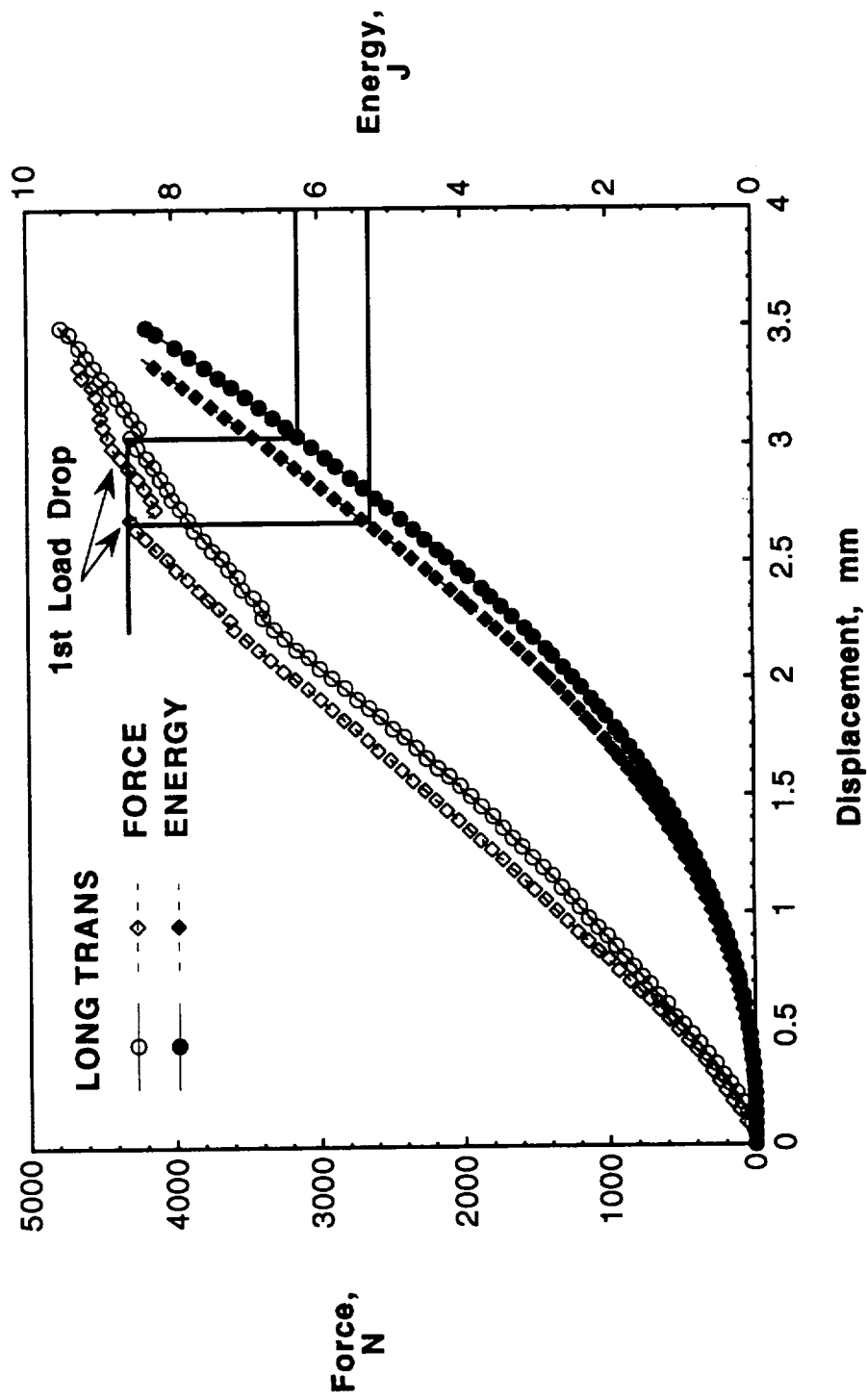
Figure 5. Comparison of the response of longitudinal and transverse [0/±45/90]s SCS-6/Timetal®21S to quasi-static indentation (QSI) tests to a nominal 8.4 J impact.

24
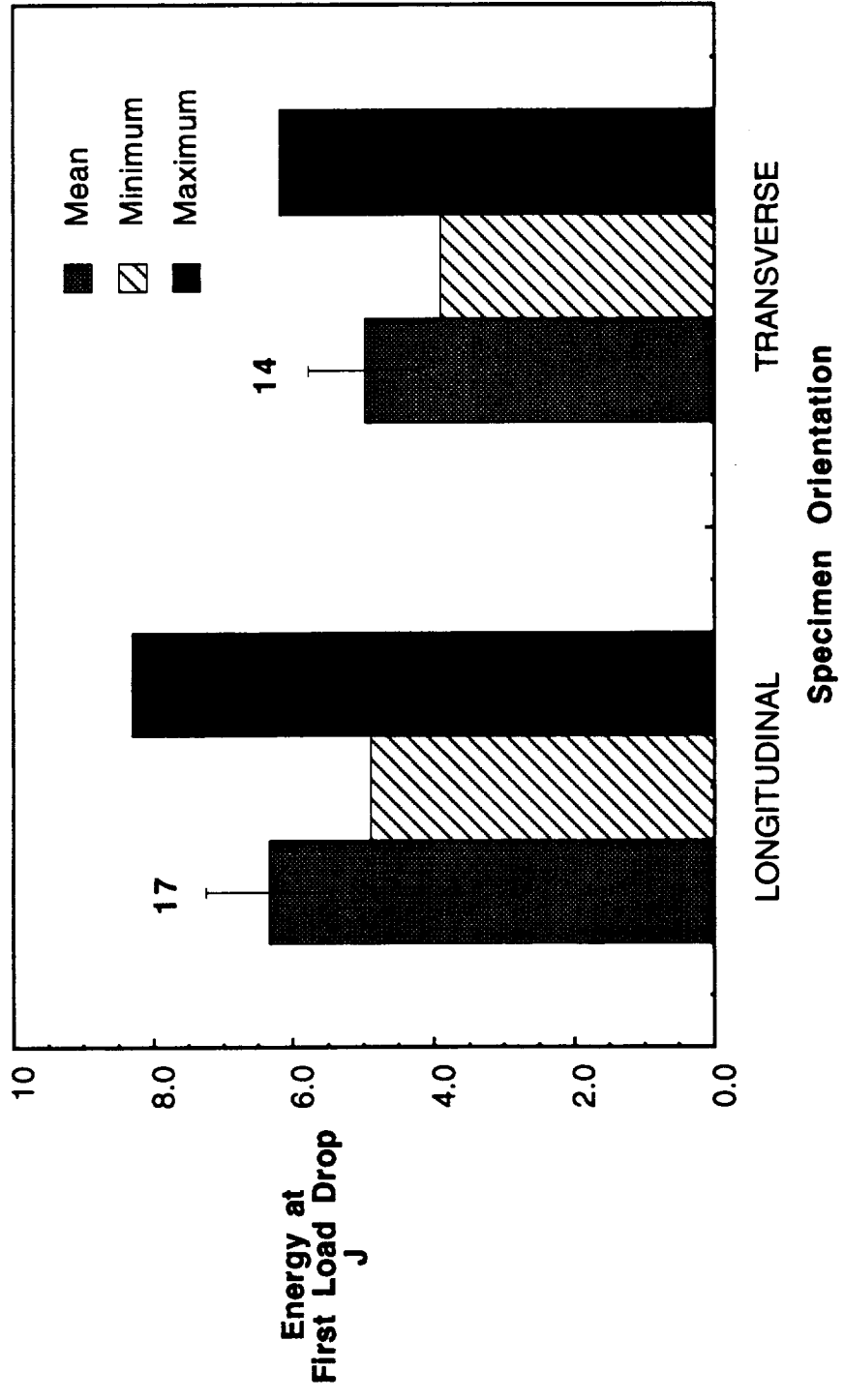
Figure 6.   Energy associated with the first load drop occurring in the force-displacement response of longitudinal and transverse specimens of [0/±45/90]s SCS-6/Timetal®21S.
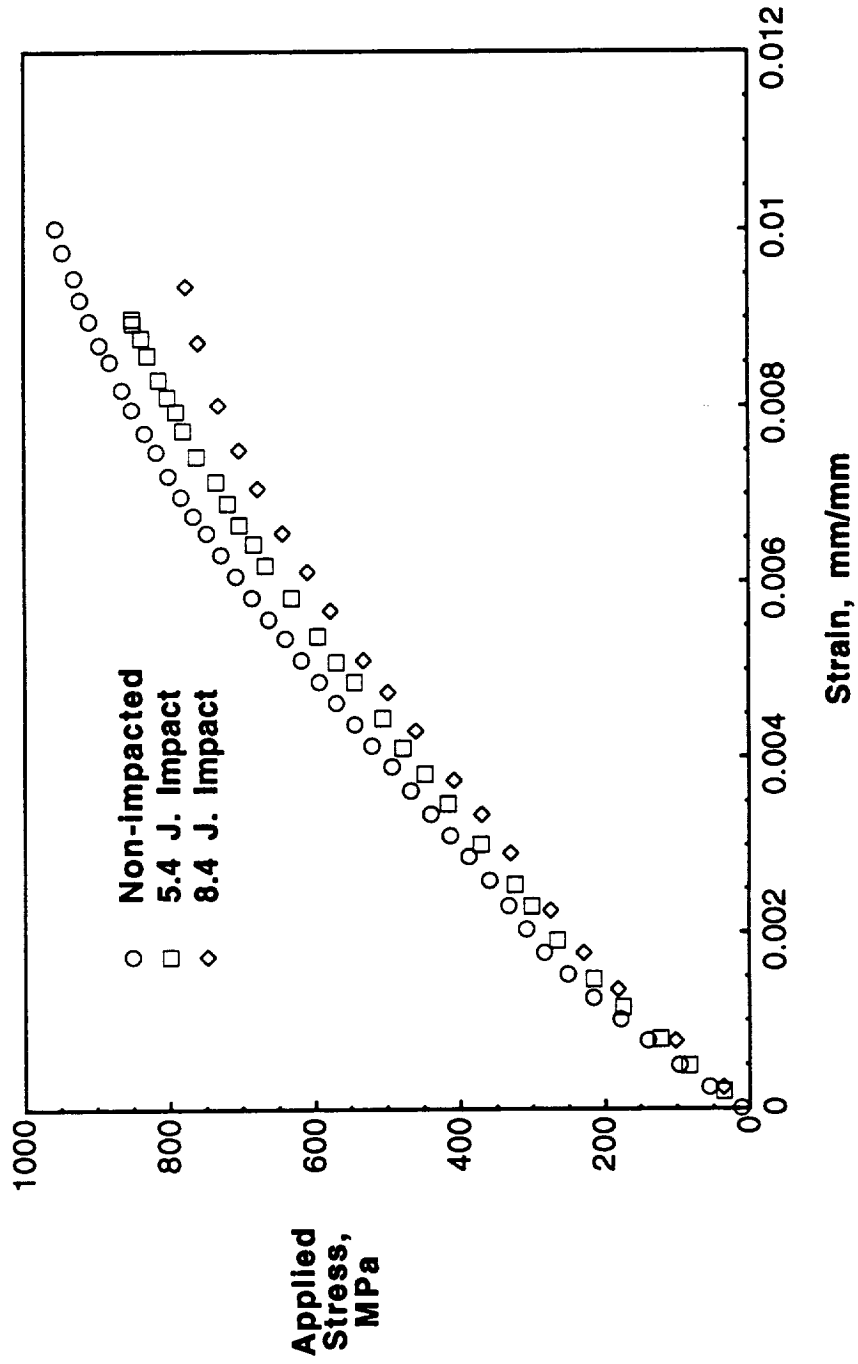
Figure 7. Applied stress versus strain response for non-impacted and impacted [0/±45/90]s SCS-6/Timetal®21S. The legend describes the nominal impact energy.
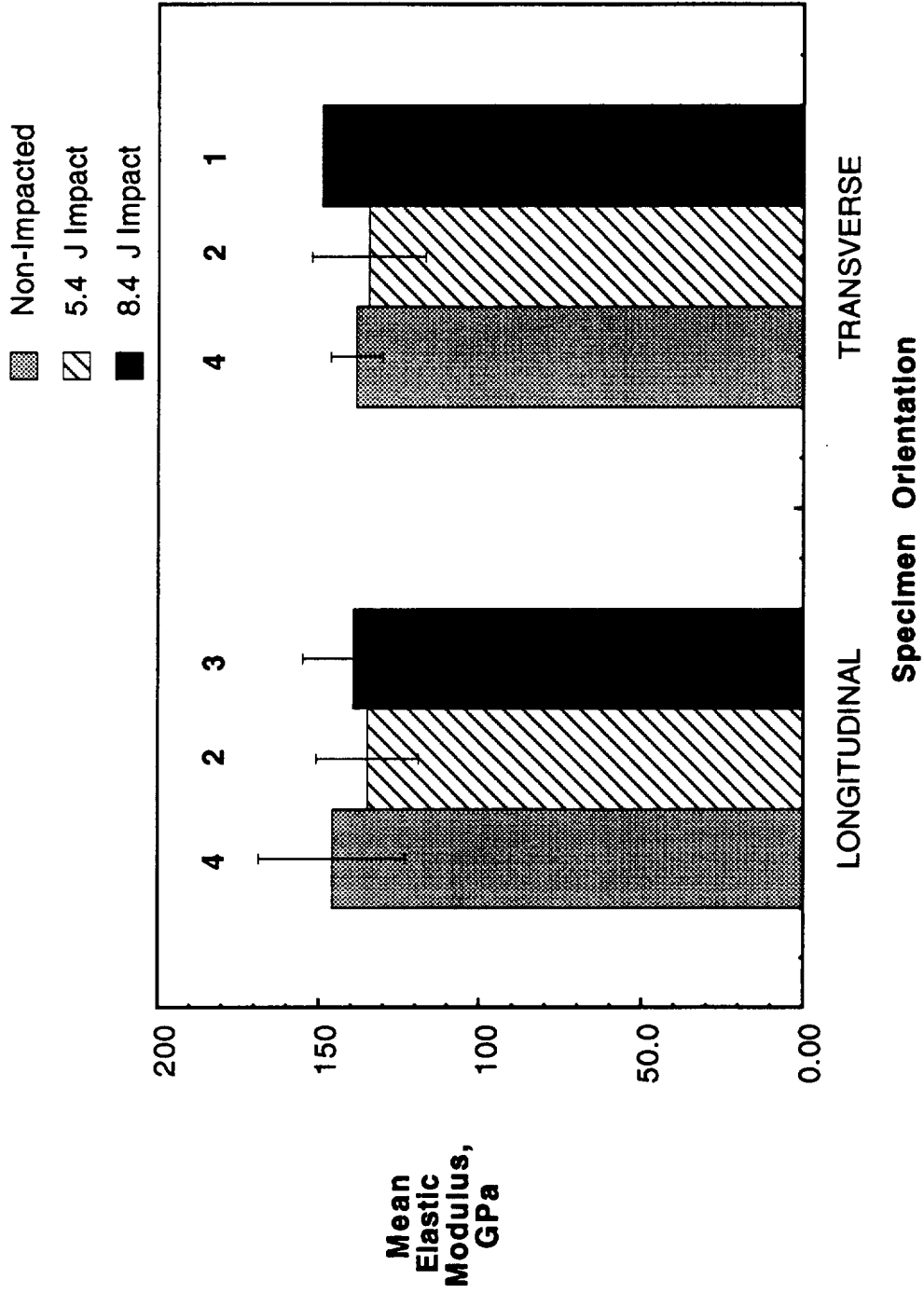
Figure 8.   Mean elastic modulus from tension tests of non-impacted and impacted [0/±45/90]s SCS-6/Timetal®21S. The legend describes the nominal impact energy.
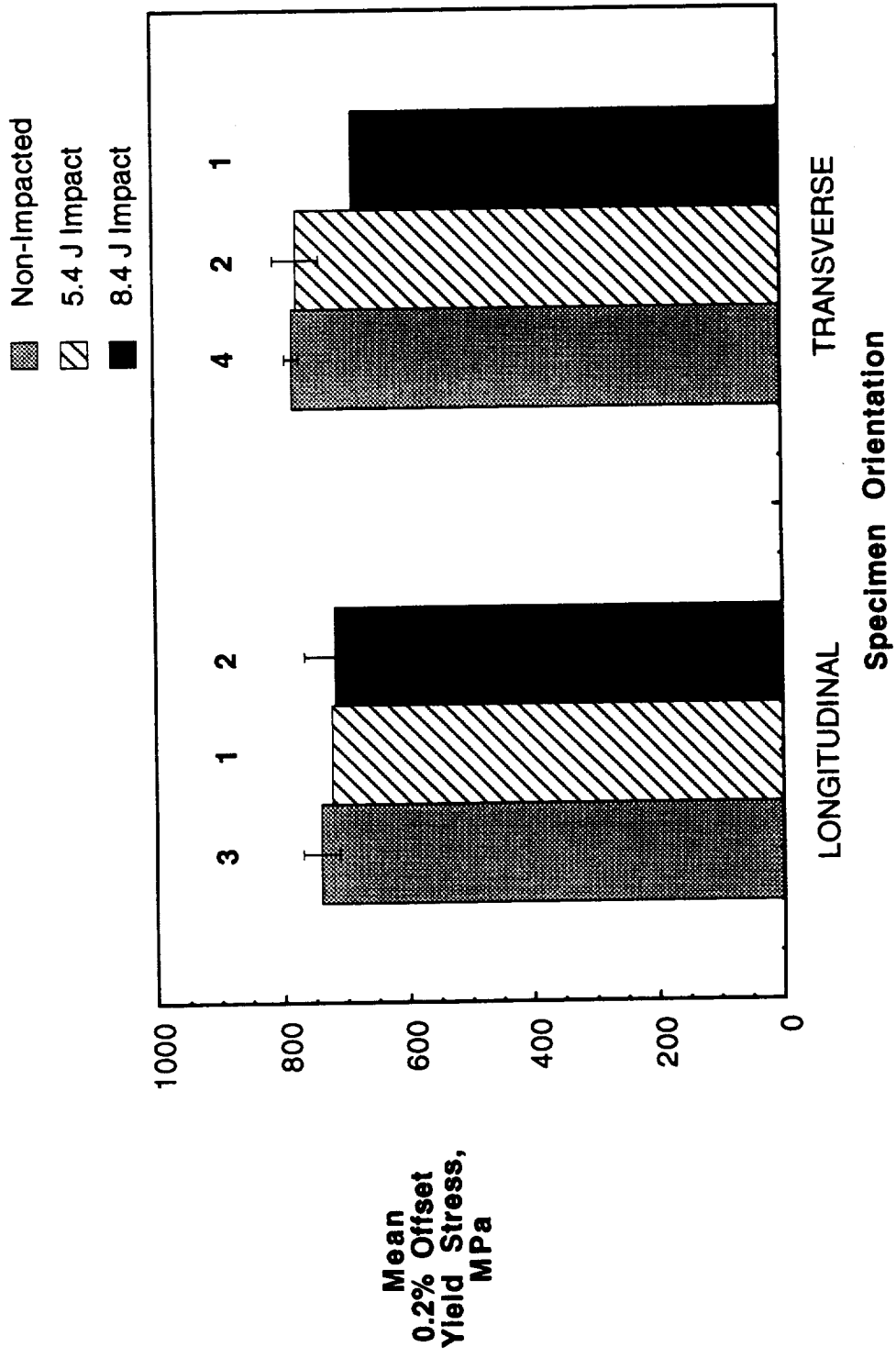
Figure 9. Mean 0.2% offset yield stress from tension tests of non-impacted and impacted [0/±45/90]s SCS-6/Timetal®21S. The legend describes the nominal impact energy.
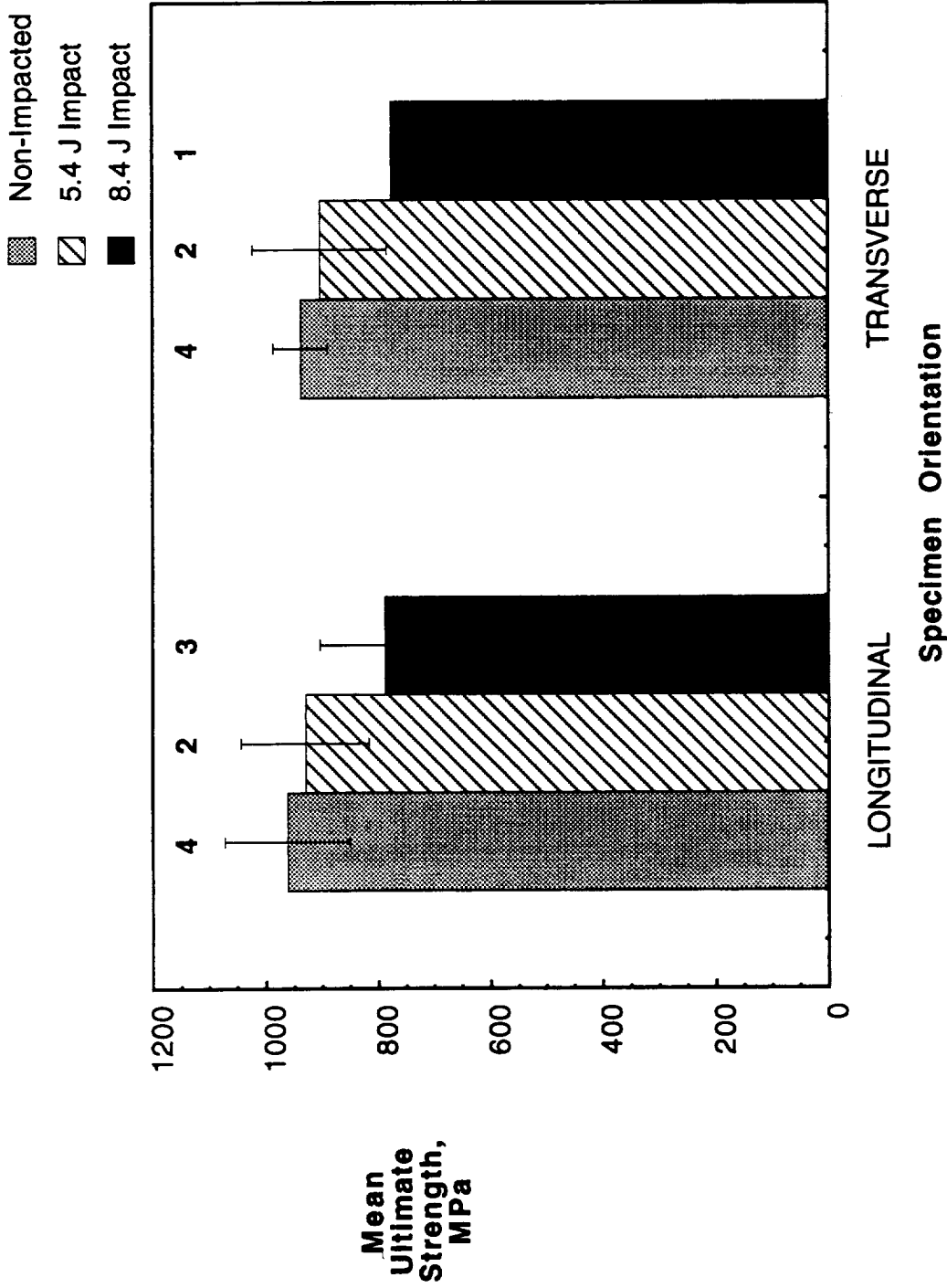
Figure 10. Mean ultimate strength from tension tests of non-impacted and impacted [0/±45/90]s SCS-6/Timetal®21S. The legend describes the nominal impact energy.
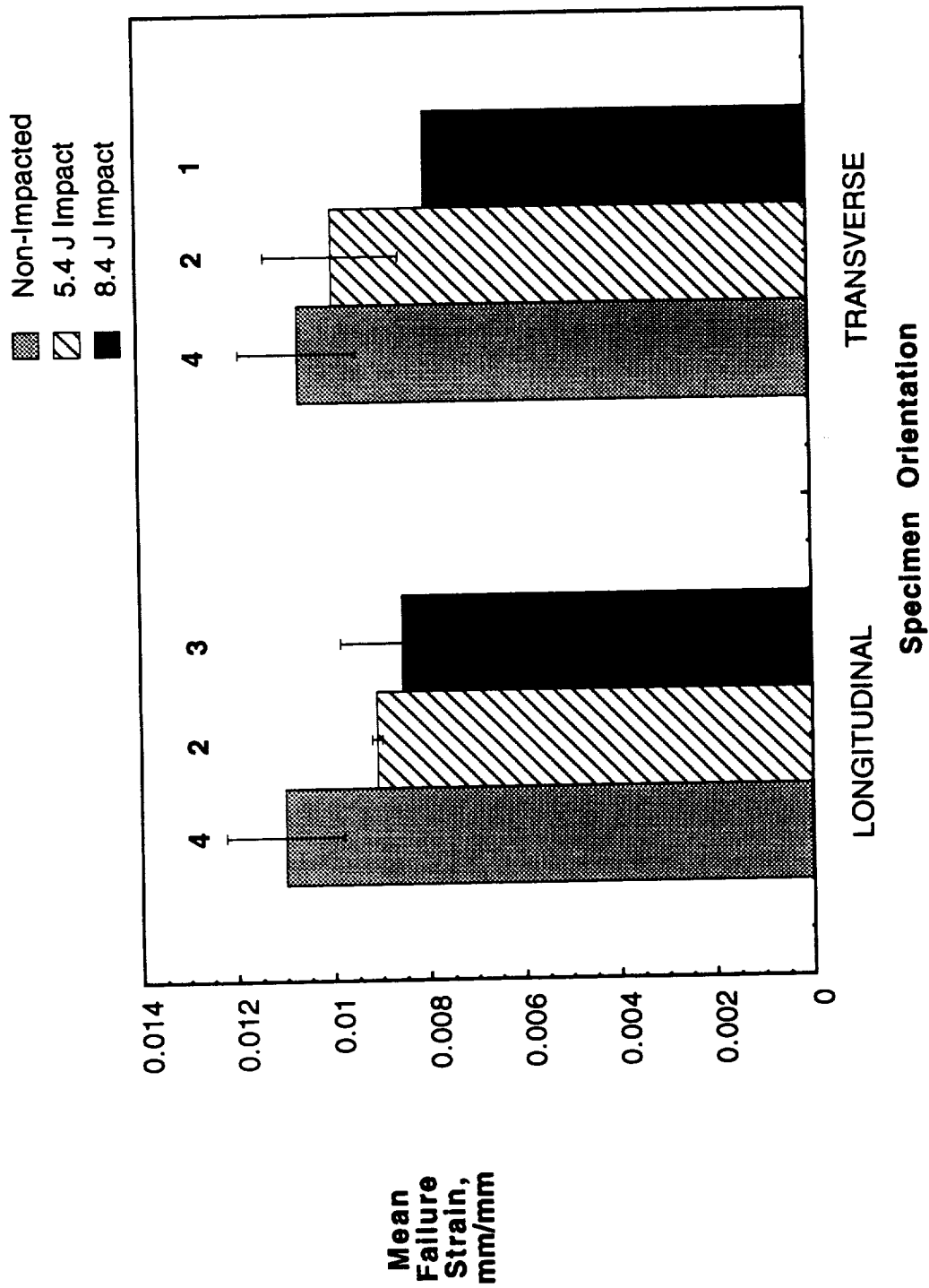
Figure 11. Mean failure strain from tension tests of non-impacted and impacted [0/±45/90]s SCS-6/Timetal®21S. The legend describes the nominal impact energy.
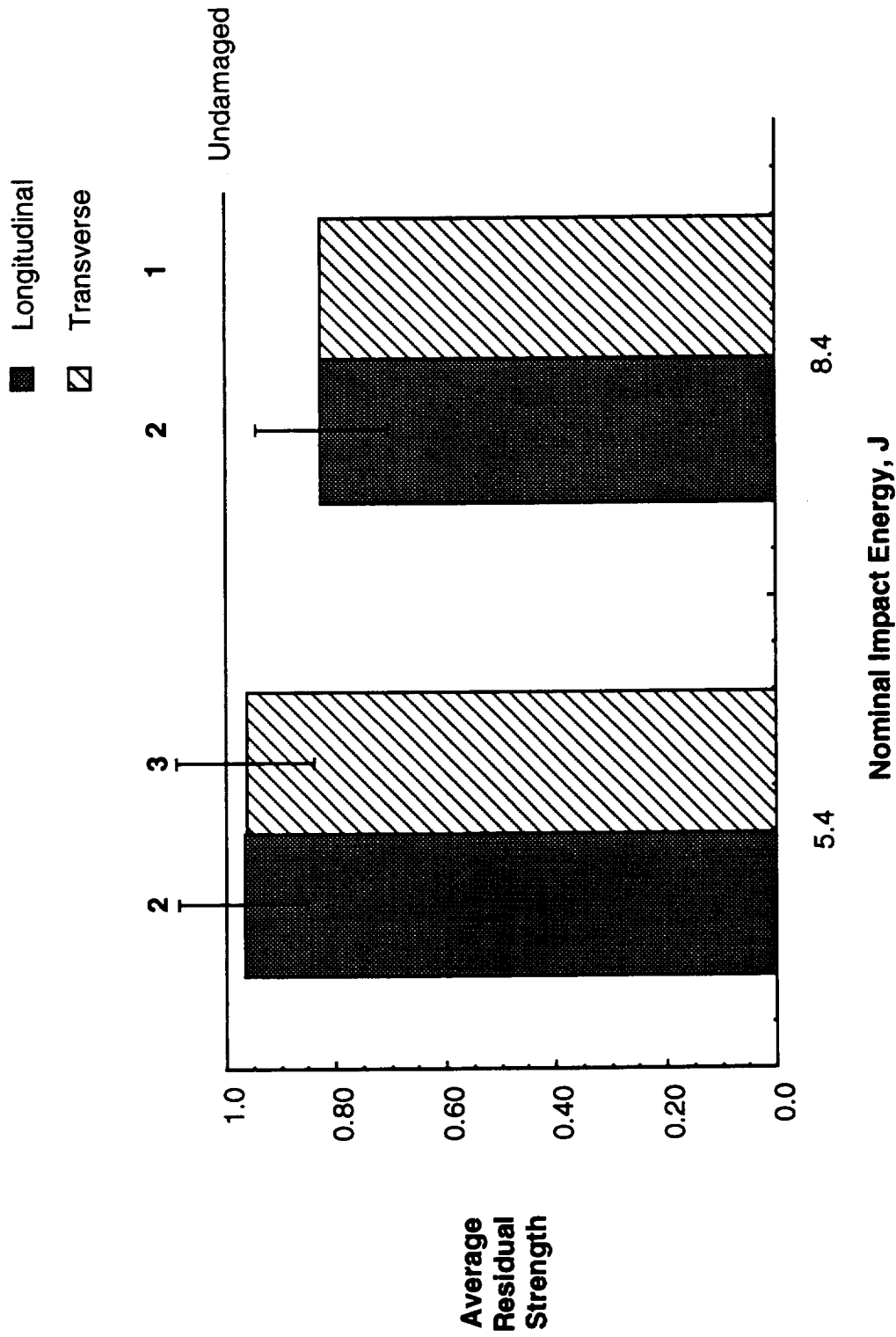
Figure 12.   Average residual tensile strength of impacted [0/±45/90]s SCS-6/Timetal®21S.   The legend describes the specimen
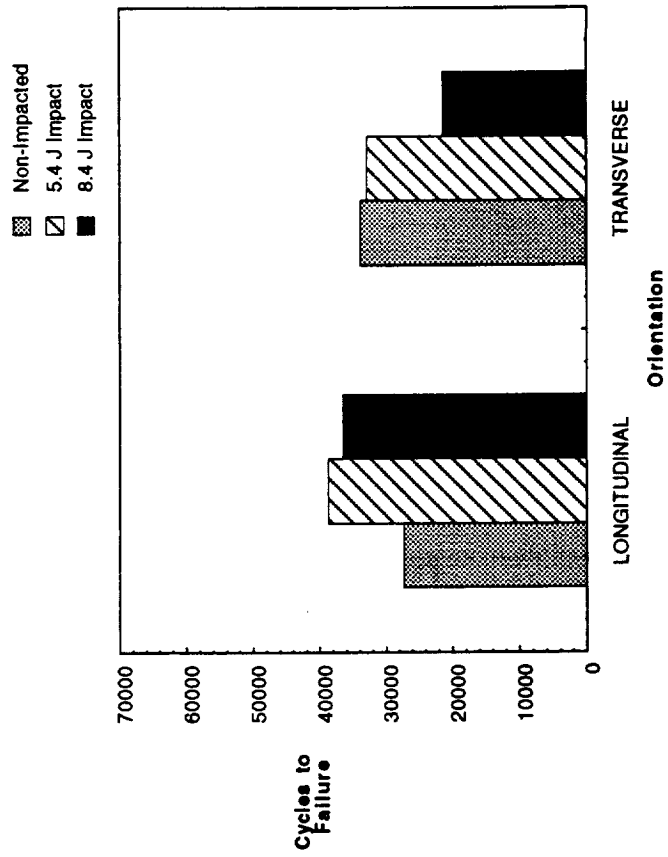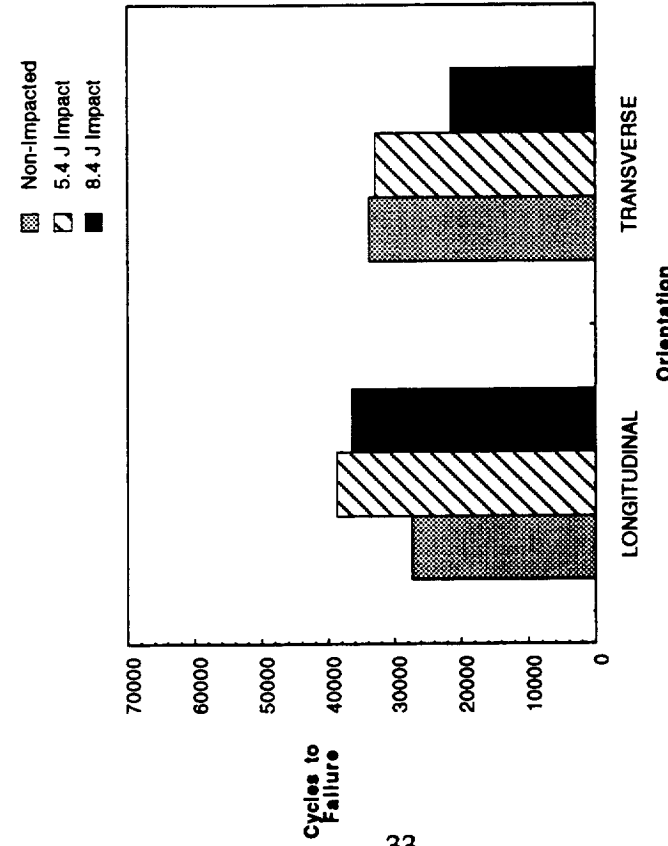orientation with respect to the 0° fiber direction.

31
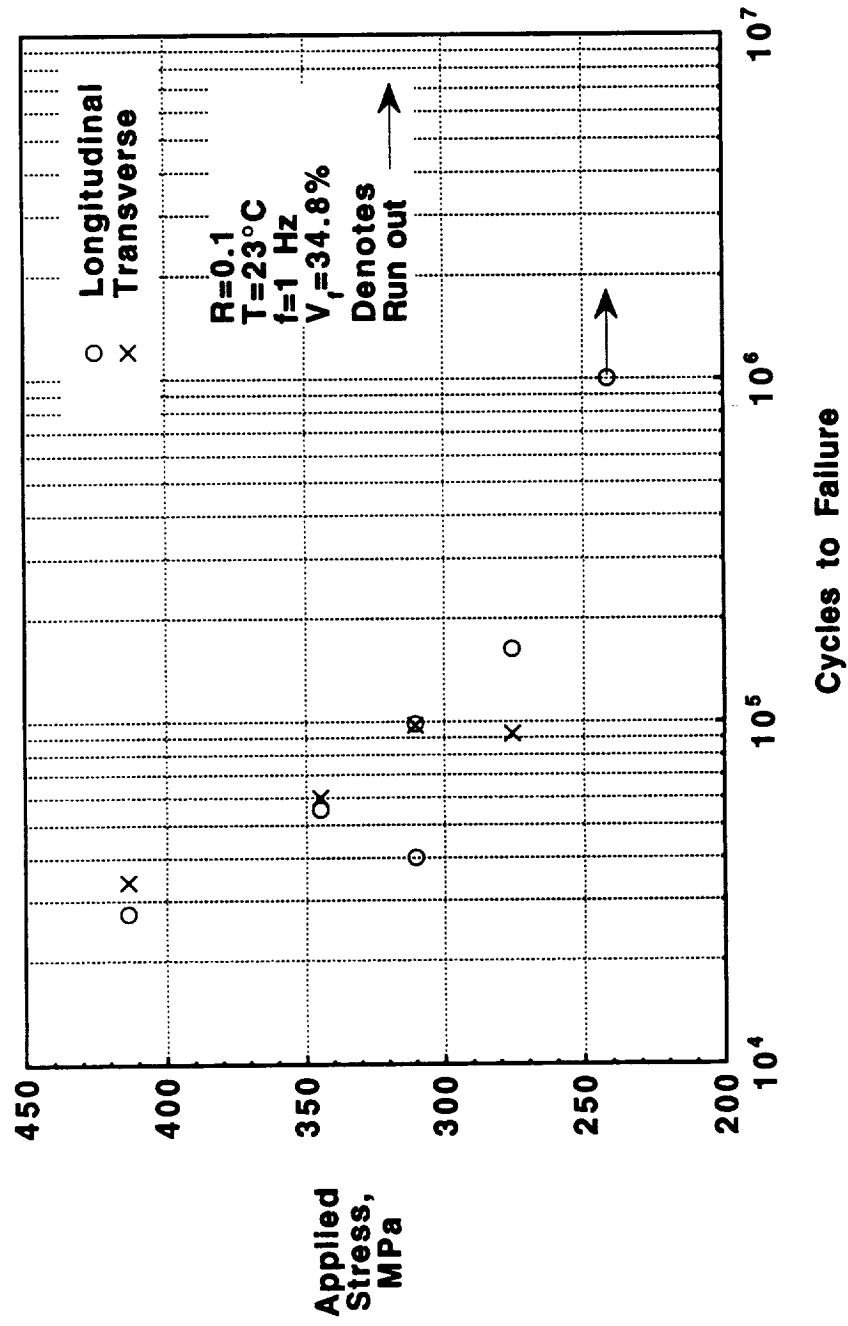
Figure 13. Applied stress versus number of cycles to failure for [0/±45/90]s SCS-6/Timetal®21S at room temperature. The legend describes the orientation of the specimen with regard to the 0° fiber direction.

(a) 345 MPa applied stress

(b) 414 MPa applied stress

Figure 14. Comparison of fatigues lives of non-impacted and impacted [0/±45/90]s SCS-6/Timetal®21S subjected to constant amplitude fatigue at two applied stress levels: a) 345 MPa and b) 414 MPa. The legends describe the nominal impact energy.
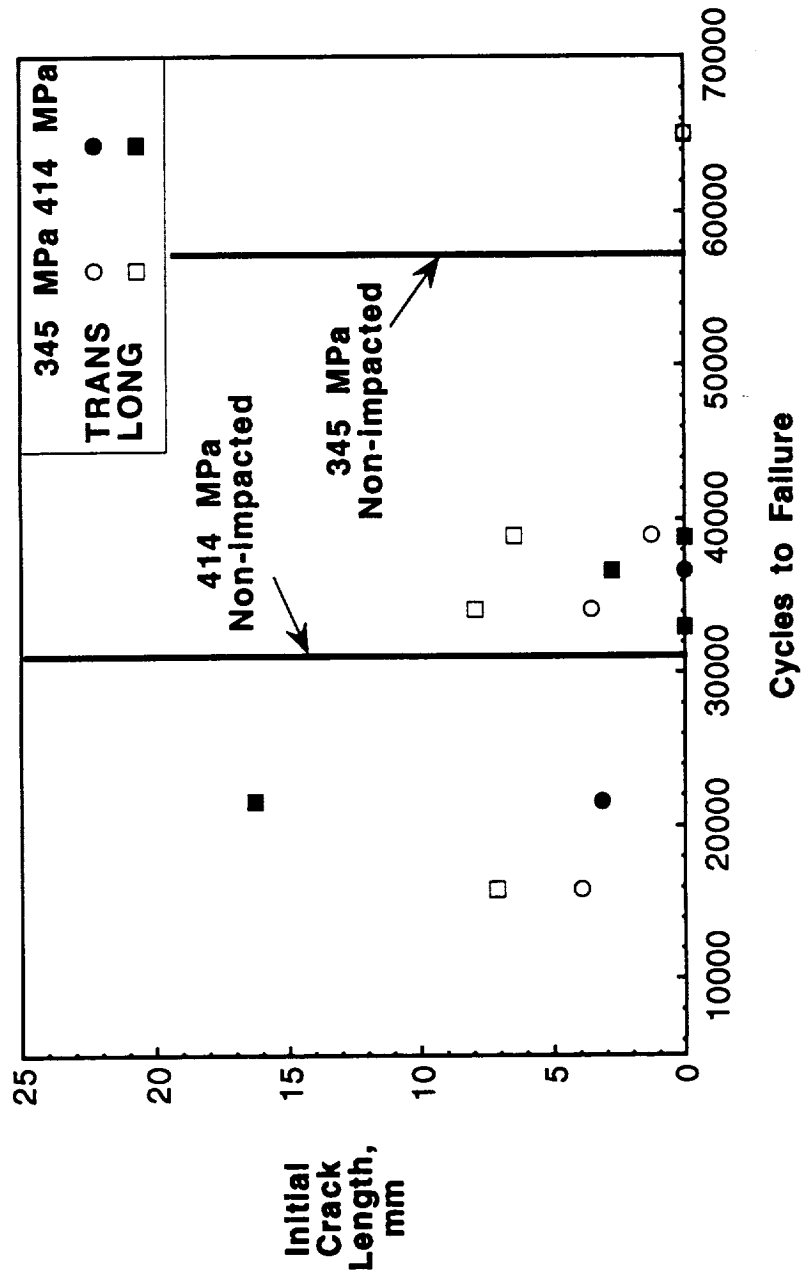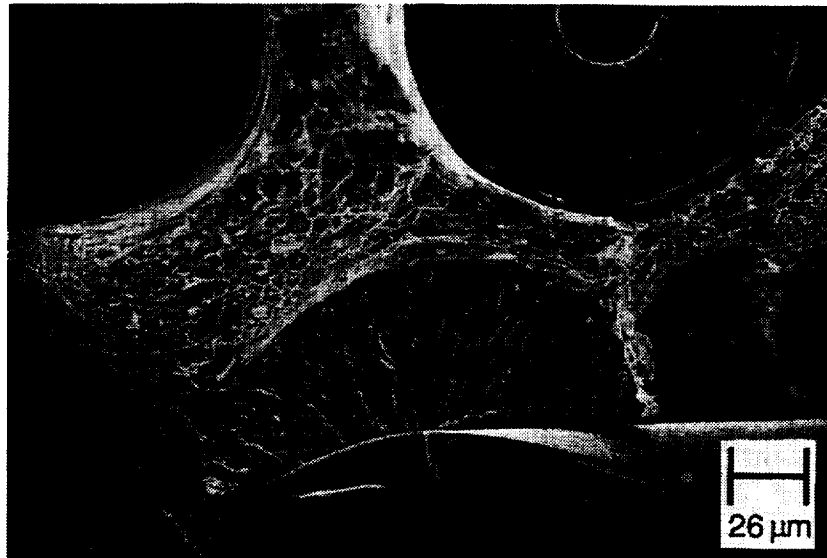
Figure 15. Longitudinal and transverse crack lengths versus number of cycles to failure for impacted [0/±45/90]s SCS-6/Timetal®21S. Solid lines represent average fatigue lives for non-impacted specimens at given applied stresses. The legend describes the specimen orientation with respect to the 0° fiber direction.

(a) Step-like fracture surface

(b) Multiple fatigue crack initiation sites

Figure 16. Fracture surface of a non-impacted $[0/\pm45/90]_S$ SCS-6/Timetal®21S subjected to constant amplitude fatigue at room temperature; a) step-like fracture surface showing fatigue crack initiation on multiple planes; b) higher magnification of a region between a $0°$ and $45°$ ply showing multiple fatigue crack initiation sites along the $45°$ fiber and ductile rupture in the matrix around the $0°$ fiber.

35
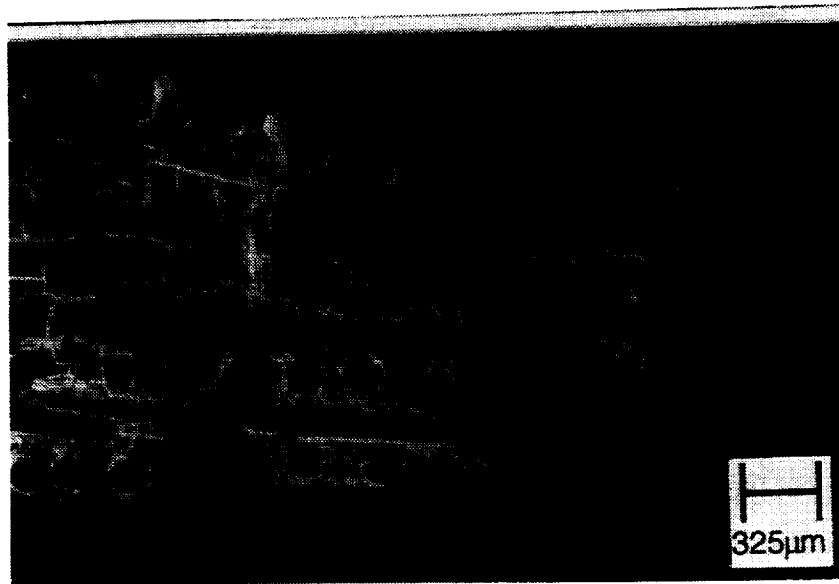
(a) Fracture surface of the impacted region
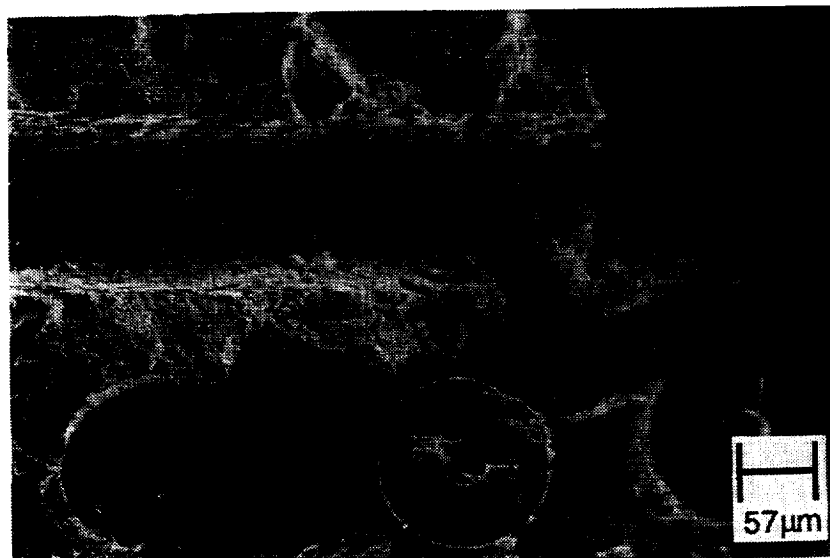
(b) Through-thickness crack

Figure 17. Fracture surface of a $[0/\pm45/90]_s$ SCS-6/Timetal®21S subjected to a nominal 8.4 J. impact and constant amplitude fatigue at room temperature; a) impacted region showing longitudinal crack on outside surface and through-thickness crack; b) magnification of the through thickness crack.

REPORT DOCUMENTATION PAGE

Public reporting burden for this collection of information is estimated to average 1 hour per response, including the time for reviewing instructions, searching existing data sources, gathering and maintaining the data needed, and completing and reviewing the collection of information. Send comments regarding this burden estimate or any other aspect of this collection of information, including suggestions for reducing this burden, to Washington Headquarters Services, Directorate for Information Operations and Reports, 1215 Jefferson Davis Highway, Suite 1204, Arlington, VA 22202-4302, and to the Office of Management and Budget, Paperwork Reduction Project (0704-0188), Washington, DC 20503.

1. AGENCY USE ONLY (Leave blank)	2. REPORT DATE May 1995	3. REPORT TYPE AND DATES COVERED Technical Memorandum

4. TITLE AND SUBTITLE

Impact Damage Resistance and Residual Property Assessment of [0/±45/90]s SCS-6/Timetal 21S

5. FUNDING NUMBERS

WU 505-63-50-04

6. AUTHOR(S)

Jennifer L. Miller, Marc A. Portanova, and W. Steven Johnson

7. PERFORMING ORGANIZATION NAME(S) AND ADDRESS(ES)

NASA Langley Research Center
Hampton, VA 23681-0001

8. PERFORMING ORGANIZATION REPORT NUMBER

9. SPONSORING / MONITORING AGENCY NAME(S) AND ADDRESS(ES)

National Aeronautics and Space Administration
Washington, DC 20546-0001

10. SPONSORING / MONITORING AGENCY REPORT NUMBER

NASA TM-110178

11. SUPPLEMENTARY NOTES

Miller: Langley Research Center, Hampton, VA; Portanova: Lockheed Martin Corporation, Hampton, VA.; Johnson: Georgia Institute of Technology, Atlanta, GA

12a. DISTRIBUTION / AVAILABILITY STATEMENT

Unclassified - Unlimited

Subject Category 24

12b. DISTRIBUTION CODE

13. ABSTRACT (Maximum 200 words)

The impact damage resistance and residual mechanical properties of [0/±45/90]s SCS-6/Timetal 21S composites were evaluated. Both quasi-static indentation and drop-weight impact tests were used to investigate the impact behavior at two nominal energy levels (5.5 and 8.4 J) and determine the onset of internal damage. Through x-ray inspection, the extent of internal damage was characterized non-destructively. The composite strength and constant amplitude fatigue response were evaluated to assess the effects of the sustained damage. Scanning electron microscopy was used to characterize internal damage from impact in comparison to damage that occurs during mechanical loading alone. The effect of stacking sequence was examined by using specimens with the long dimension of the specimen both parallel (longitudinal) and perpendicular (transverse) to the 0° fiber direction. Damage in the form of longitudinal and transverse cracking occurred in all longitudinal specimens tested at energies greater than 6.3 J. Similar results occurred in the transverse specimens tested above 5.4 J. Initial load drop, characteristic of the onset of damage, occurred on average at 6.3 J in longitudinal specimens and at 5.0 J in transverse specimens. X-ray analysis showed broken fibers in the impacted region in specimens tested at the higher impact energies. At low impact energies, visible matrix cracking may occur, but broken fibers may not. Matrix cracking was noted along fiber swims and it appeared to depend on the surface quality of composite. At low impact energies, little damage has been incurred by the composite and the residual strength and residual life is not greatly reduced as compared to an undamaged composite. At higher impact energies, more damage occurred and a greater effect of the impact damage was observed.

14. SUBJECT TERMS

Metal matrix composites; Impact; Damage; Residual strength; Residual fatigue

15. NUMBER OF PAGES

37

16. PRICE CODE

A03

17. SECURITY CLASSIFICATION OF REPORT Unclassified	18. SECURITY CLASSIFICATION OF THIS PAGE Unclassified	19. SECURITY CLASSIFICATION OF ABSTRACT	20. LIMITATION OF ABSTRACT